Published in final edited form as:
Biomaterials. 2011 December ; 32(36): 9584–9593. doi:10.1016/j.biomaterials.2011.09.006.

Synergistic regulation of cell function by matrix rigidity and adhesive pattern

Shinuo Weng[1] and **Jianping Fu**[1,2,*]

[1]Department of Mechanical Engineering, University of Michigan, Ann Arbor, MI 48109, USA

[2]Department of Biomedical Engineering, University of Michigan, Ann Arbor, MI 48109, USA

Abstract

Cell-extracellular matrix (ECM) interactions play a critical role in regulating cellular behaviors. Recent studies of cell-ECM interactions have mainly focused on the actomyosin based and adhesion mediated mechanosensing pathways to understand how individual mechanical signals in the cell microenvironment, such as matrix rigidity and adhesive ECM pattern, are sensed by the cell and further trigger downstream intracellular signaling cascades and cellular responses. However, synergistic and collective regulation of cellular behaviors by matrix rigidity and adhesive ECM pattern are still elusive and largely uncharacterized. Here, we generated a library of microfabricated polydimethylsiloxane (PDMS) micropost arrays to study the synergistic and independent effects of matrix rigidity and adhesive ECM pattern on mechanoresponsive behaviors of both NIH/3T3 fibroblasts and human umbilical vein endothelial cells (HUVECs). We showed that both cell types were mechanosensitive and their cell spreading, FA formation, cytoskeletal contractility, and proliferation were all strongly dependent on both substrate rigidity and adhesive ECM pattern. We further showed that under the same substrate rigidity condition, smaller and closer adhesive ECM islands would cause both cells to spread out more, form more adhesion structures, and have a higher proliferation rate. The influence of adhesive ECM pattern on rigidity-mediated cytoskeletal contractility was cell type specific and was only significant for NIH/3T3. Morphometric analysis of cell populations revealed a strong correlation between focal adhesion and cell spreading, regardless of substrate rigidity and adhesive ECM pattern. We also observed a strong correlation between cellular traction force and cell spreading, with a substantially smaller independent effect of substrate rigidity on traction force. Our study here had determined key aspects of the biomechanical responses of adherent cells to independent and collective changes of substrate rigidity and adhesive ECM pattern.

Keywords

Extracellular matrix (ECM); Matrix rigidity; Adhesive pattern; Polydimethylsiloxane (PDMS); Mechanotransduction

[*]Correspondence should be addressed to J. Fu [J. Fu (jpfu@umich.edu, Tel: 01-734-615-7363, Fax: 01-734-647-7303)].

INTRODUCTION

Environmental sensing to external signals is widespread in almost every cell type, from prokaryotes to multicellular organisms. Cells sense, analyze and integrate these external signals, both chemical and physical, and subsequently change its morphology, dynamic behaviors, and eventually, fate. For adherent cells to grow and function, it is crucial for them to maintain their tight association with the diverse connective tissue components that form the extracellular matrix (ECM). In recent years, it has become increasingly apparent that the cellular responses to microenvironmental signals go far beyond the ability of the cells to chemically sense specific ECM ligands, and it encompasses a wide range of physical cues that are generated at, or acted on the adhesive interface between the cells and the surrounding matrix [1–5]. Numerous studies have demonstrated the capacity of cells to respond to changes in multiple biointerfacial parameters, including adhesive ligand density and pattern [6–8], surface compliance (or ECM rigidity) [9–15], and ECM dimensionality and anisotropy [16–18], among other characteristics. It is generally believed that the cellular sensory machinery is capable of integrating this complex information into a coherent environmental signal, by globally altering cell shape and actin cytoskeletal organization [3, 19–21], and by locally modulating adhesion formation and signaling [1, 2, 4].

Conventional methods to study cell-ECM interactions have largely relied on natural and synthetic hydrogels [5, 22, 23]. Although these hydrogel systems have proven important to deepen our understanding of cellular sensing of environmental signals, they still suffer from certain limitations that prevent their applications in some detailed investigations of biointerfacial cellular phenomena [3, 22, 23]. For example, conventional methods using hydrogels derived from natural ECM proteins (such as collagen-I, fibrin, and Matrigel) are known to have difficulty controlling their bulk mechanical properties. Further, in these natural hydrogels, changes in gel stiffness cannot be decoupled from other parameters such as ligand density or gel fiber thickness. The synthetic hydrogel systems such as polyacrylamide (PA) or polyethylene glycol (PEG) gels present a significant advancement for studies of cell-ECM interactions [14, 24, 25], as they have well-defined bulk mechanical properties and are chemically inert and can be functionalized with adhesive peptides and proteins using linker chemistry. Yet, these synthetic hydrogel systems are still not immune to molecular-scale changes in porosity, wettability, hydration, polymer chain mobility and binding properties of immobilized adhesive ligands that accompany changes in their bulk stiffness [3, 23]. It has been shown that these molecular-scale changes can have their profound independent effects on cellular functions [26–28]. For example, a very recent study using synthetic hydrogels for human pluripotent stem cells indicates that these molecular-scale changes in wettability and surface topology can have significant effects on stem cell survival and cloning efficiency [26]. There are other reports that clearly suggest that the nanoscale local alterations in receptor-ligand binding characteristics could strongly influence cellular sensing of ECM surface properties and thus downstream cellular behaviors [27, 28].

The importance of development of new tools for investigating biointerfacial cellular phenomena has been well recognized and documented [23, 29, 30]. Although the natural and synthetic hydrogel systems discussed above will continue to be important in characterizing

and controlling cell-material interactions, there is a great current need for new classes of synthetic materials in which surface chemistry, adhesive pattern, topography, and mechanics can be independently controlled to facilitate the quest for design principles and material selection rules to control cellular responses. Recently, our group and some others have proposed an idea to use microfabricated elastomeric polydimethylsiloxane (PDMS) micropost arrays to regulate substrate rigidity independently of effects on adhesive and other material surface properties [31, 32]. Our approach involves a library of replica-molded arrays of hexagonally spaced PDMS microposts from microfabricated silicon masters, which present the same surface geometry but different post heights to control substrate rigidity. The spring constant K of the PDMS micropost is solely determined by its geometry and by the *Young*'s modulus E of PDMS, and K can be approximately calculated using the *Euler-Bernoulli* beam theory as $K=3\pi ED^4/(64L^3)$ [32–34], where D and L are the PDMS post diameter and height, respectively. The substrate rigidity of the PDMS micropost array can be further characterized using an effective *Young*'s modulus E_{eff} of a continuous elastic substrate, and E_{eff} is calculated using the expression of $E_{eff} = 9K/(2\pi D)$ [32]. Thus, the rigidity of the PDMS micropost array can be modulated simply by varying the post height L and diameter D while keeping all other aspects of the substrate such as surface chemistry, ligand density, and bulk and nanoscale mechanics of the PDMS unchanged. In our previous study, we have shown that indeed, the rigidity of the PDMS micropost array can significantly impact cell morphology, focal adhesion (FA) formation, cytoskeletal contractility, and stem cell differentiation [31, 35].

Most of the existing biomechanics studies characterizing biointerfacial cellular phenomena, including our own previous report examining the PDMS micropost array, have focused on determining how individual biophysical parameters in the cell microenvironment, such as substrate rigidity and adhesive ECM pattern, are sensed by cells and further trigger downstream intracellular signaling cascades and cellular responses. Thus, synergistic and collective regulations of cellular behaviors by a combination of different biointerfacial parameters are still elusive and largely uncharacterized, which will clearly hamper future efforts to design efficient synthetic materials and biointerfaces containing multiple biophysical signals to collectively direct cellular behaviors. The current incomplete understanding of cell-ECM interactions is largely due to the limited number of experimental techniques and approaches that can precisely and independently regulate multiple biointerfacial parameters simultaneously in the same experimental system. In this work, to specifically address this technical limitation and thus advance our current understanding of the combined influences of different biointerfacial parameters on cellular behaviors, we took advantage of the unique characteristic of the PDMS micropost array where the mechanical rigidity of the PDMS micropost array could be easily and completely decoupled from its surface properties including ECM ligand density and presentation and adhesive ECM pattern. In this work, we specifically studied the synergistic and independent effects of matrix rigidity and adhesive ECM pattern on cell spreading, FA formation, cytoskeletal contractility, and proliferation for different types of adherent mammalian cells.

MATERIALS AND METHODS

Fabrication of PDMS micropost array

Elastomeric PDMS micropost arrays were fabricated using conventional semiconductor microfabrication techniques and replica molding, as previously described [31, 35]. Briefly, silicon micropost array masters were fabricated using high-resolution projection photolithography and deep reactive ion-etching (DRIE) techniques. By controlling the mask design of the micropost array structure and the DRIE etch time, we could determine precisely different geometrical factors of the silicon micropost array master, including post diameter, post center-to-center (c.t.c) distance, and post height. These silicon masters were silanized with (tridecafluoro-1,1,2,2,-tetrahydrooctyl)-1-trichlorosilane (United Chemical Technologies, Bristol, PA) for 4 hrs under vacuum to aid subsequent release of the negative PDMS (Sylgard 184, Dow- Corning, Midland, MI) mold from the silicon master. The PDMS micropost array was then generated by replica molding. In brief, 1:10 (w/w, curing agent:base) ratio PDMS prepolymer was poured over the silicon micropost master, cured at 110°C for 20 min, peeled off, oxidized with air plasma for 1 min (~200 mTorr; Plasma Prep II, West Chester, PA), and silanized with (tridecafluoro-1,1,2,2,-tetrahydrooctyl)-1-trichlorosilane vapor for 40 hrs to obtain the PDMS negative mold. To generate the final PDMS micropost array, 1:10 ratio PDMS prepolymer was poured over the negative PDMS mold, degassed under vacuum, cured at 110°C for 40 hrs, and peeled off the negative mold. When peeling induced collapse of the PDMS microposts, we regenerated the free-standing PDMS microposts by sonication in 100% ethanol for 30 sec followed by dry-release with liquid CO_2 using a critical point dryer (Samdri®-PVT-3D, Tousimis, Rockville, MD). Geometries of the silicon post master and PDMS micropost array were examined under optical microscopy and were further characterized using a surface profilometer (Prometrix P-10, KLA-Tenco Co., CA) and scanning electron microscopy (JEOL6320FV, JEOL USA, Inc., Peabody, MA).

Mechanical characterization of PDMS micropost array

The commercial finite element analysis (FEA) suite ABAQUS (SIMULIA, Dassault Systèmes) was used to analyze the nominal spring constant K of the PDMS micropost, as described previously [31]. The PDMS micropost was modeled as a neohookian hyperelastic cylinder with a *Young*'s modulus E of 2.5 MPa, and was discretized into hexahedral mesh elements. The bottom surface of the PDMS micropost was fixed in all degrees of freedom. A horizontal load F was then applied uniformly at all of the nodes on the top of the micropost. FEA analysis was performed to determine displacement δ of the micropost top due to F. From the force (F)-displacement (δ) curve, the nominal spring constant K of the PDMS micropost was computed by linearly extrapolating F to zero post deflection δ as $K = dF/d\delta$ ($\delta \rightarrow 0$). For our comparative studies for the two sets of PDMS micropost arrays with different post diameters (*D(0.8) vs. D*(1.83)), we further converted the nominal spring constant K of the PDMS micropost into an effective *Young*'s modulus E_{eff} of a continuous elastic substrate, using the expression of $E_{eff} = 9K/(2\pi D)$ [32]. The two sets of PDMS micropost arrays reported in this work (*D(0.8)* and *D*(1.83)) produced a more than 10,000-fold range of rigidity from 0.10 kPa (*D*(0.8)*L*(0.42)) to 1,200 kPa (*D*(0.8)*L*(13.45)) (Fig. 1e).

Surface functionalization of PDMS micropost array and flat PDMS surface

As described previously [31, 35], we used microcontact printing to functionalize the top of the PDMS micropost with ECM proteins to promote cell attachment. Briefly, a flat 1:30 PDMS stamp was prepared and inked with fibronectin (BD Biosciences, San Jose, CA) at a saturating concentration of 50 μg mL^{-1} in distilled water for 1 hr at room temperature. The PDMS stamp was then thoroughly rinsed with distilled water and blown dry with a stream of nitrogen. In parallel, the PDMS micropost array was treated with ultraviolet (UV) ozone (UV-ozone cleaner; Jelight, Irvine, CA) for 7 min to oxidize the PDMS surface, which resulted in the PDMS surface changing from hydrophobic to hydrophilic, allowing complete transfer of ECM proteins from the PDMS stamp to the top of the PDMS micropost. The PDMS stamp was then placed in conformal contact with the PDMS micropost array for about 5 sec to complete the protein transfer process. Pluronics F127 NF dissolved in PBS (0.2%, w/v; BASF, Ludwigshafen, Germany) was then adsorbed to the PDMS surface for 1 hr at room temperature to prevent protein adsorption to non-functionalized portions of the PDMS micropost array. To utilize the PDMS micropost array for live-cell traction force measurement, we performed an additional labeling step to stain the PDMS micropost with 1,1'-dioleyl-3,3,3',3'-tetramethylindocarbocyanine methanesulfonate (Δ^9-DiI; Invitrogen, Carlsbad, CA) before adding pluronics F 127NF on the PDMS micropost array.

For microcontact stamp-off [36], flat 1:30 and 1:10 PDMS substrates were prepared by curing the PDMS prepolymer at 110°C for 48 hrs and then inked with fibronectin at 50 μg mL^{-1} in distilled water for 30 min, rinsed with distilled water, and blown dry under nitrogen. In parallel, a 1:10 negative PDMS mold was cast against the silicon micropost master and then surface-oxidized with a UV ozone treatment for 7 min. The negative PDMS mold was placed in conformal contact with the fibronectin-coated flat PDMS substrate, to completely remove fibronectin in direct contact with the negative PDMS stamp. The flat PDMS substrate was then incubated with 0.2% Pluronics F127 NF for 1 hr to prevent protein adsorption to non-functionalized portions of the flat PDMS substrate. Efficiency of the microcontact stamp-off method was confirmed using Alexa Fluor 555 conjugated bovine serum albumin (BSA). After microcontact stamp-off, fluorescence signal outside of the BSA circle patterns on the flat PDMS substrate was not detectable (Fig. 2b&c), confirming complete protein removal with microcontact stamp-off.

Cell culture and reagents

NIH/3T3 mouse embryonic fibroblasts (ATCC, Manassas, VA) were maintained in the growth medium consisting of high-glucose Dulbecco's modified Eagle's medium (DMEM; Invitrogen) supplemented with 10% bovine serum (Atlanta Biological, Atlanta, GA), 100 μg mL^{-1} L-glutamine, 100 units mL^{-1} penicillin, and 100 μg mL^{-1} streptomycin. Human umbilical vein endothelial cells (HUVECs; Lonza, Walkersville, MD) were grown in the endothelial cell growth medium-2 (Clonetics EGM-2; Lonza), and were maintained on gelatin-coated tissue culture polystyrene. Early passages of HUVECs were used in experiments (passage 4–7). Fresh 0.25% and 0.05% trypsin-EDTA in PBS was used to re-suspend NIH/3T3 and HUVECs, respectively. NIH/3T3 and HUVECs were seeded at a low density (4,000 cells cm^{-2}) in the growth medium onto the PDMS micropost array or flat PDMS substrates, and were then allowed to spread out overnight before other assays.

Immunofluorescence staining and EdU proliferation assay

Immunofluorescence staining of FAs was performed as previously described [31, 37]. In brief, cells were incubated in an ice-cold cytoskeleton buffer (50 mM NaCl, 150 mM sucrose, 3 mM $MgCl_2$, 1 μg mL^{-1} aprotinin, 1 μg mL^{-1} leupeptin, and 1 μg mL^{-1} pepstatin) for 1 min, followed by the cytoskeleton buffer supplemented with 0.5% Triton X-100 (Roche Applied Science, Indianapolis, IN) for 1 min. Detergent-extracted cells were fixed with 4% paraformaldehyde (Electron Microscopy Science, Hatfield, PA) in PBS, washed with PBS, incubated with 10% goat serum (Invitrogen) and then a primary antibody to vinculin produced in mouse (Sigma-Aldrich, St. Louis, MO), and stained with Alexa Fluor 488 conjugated goat anti-mouse IgG secondary antibody (Invitrogen). To visualize F-actin and nucleus, Alexa Fluor 555 conjugated phalloidin (Invitrogen) and 4',6-diamidino-2-phenylindole (DAPI; Invitrogen) were used.

For the EdU cell proliferation assay, NIH/3T3 cells were first starved at confluence in the growth medium supplemented with 0.5% bovine serum for 48 hrs to synchronize cell cycle before trypsinization. For HUVECs, cells were starved at confluence in EBM-2 supplemented with 0.1% FBS for 24 hrs before trypsinization. Synchronized cells were re-plated on the PDMS micropost array or flat PDMS substrates and recovered in the complete growth medium for 12 to 24 hrs, and were then exposed to 4 μM 5-ethynyl-2'-deoxyuridine (EdU; Invitrogen) in the growth medium for a desired period of time (9 hrs for NIH/3T3 and 24 hrs for HUVECs). Cells were then fixed with 3.7% formaldehyde in PBS (Electron Microscopy Science), permeabilized with 0.5% Triton X-100 in PBS, washed with 10% goat serum, stained with Alexa Fluor 488 conjugated azide targeting the alkyne groups in the EdU that was incorporated in the newly synthesized DNA. The cells were co-stained with Hoechst 33342 (Invitrogen) to visualize cell nucleus.

Quantitative analysis of cell spread area and focal adhesion

Cell spread area and focal adhesion (FA) formation were quantified as described previously [31, 38]. In brief, immunostaining images of the F-actin cytoskeleton and vinculin were collected for each cell using a 40× objective (1.3 NA, oil immersion, EC Plan NEOFLUAR; Carl Zeiss MicroImaging, Thornwood, NY) on a Zeiss Observer.Z1 microscope (Carl Zeiss MicroImaging) attached with a thermoelectrically-cooled monochrome charge-coupled device (CCD) camera (AxioCam HRM, Carl Zeiss MicroImaging). Images obtained by Axiovision (Carl Zeiss MicroImaging) were processed using custom-developed MATLAB programs (Mathworks, Natick, MA). To determine the spread area for each cell, a black and white cell image was generated from the image overlay of fluorescently-stained F-actin and vinculin, and the resultant white pixels were summed to quantify cell area. More specifically, the Canny edge detection method was used to binarize the actin fibers and FAs, and then image dilation, erosion, and fill operations were used to fill in the gaps between the white pixels. To quantify FA number and area for each cell, the grayscale vinculin image was thresholded to produce a black and white FA image from which the white pixels, representing FAs, were counted and summed.

Quantification of cell contractility

Cell contractility was quantified as previously described [31, 35]. In brief, Δ^9-DiI-stained PDMS microposts underlying the adherent cells were imaged at the focal plane passing through the top surface of the unbent posts with a 40× objective (1.3 NA, oil immersion; EC Plan NEOFLUAR; Carl Zeiss MicroImaging) on a Zeiss Observer.Z1 microscope attached with a thermoelectrically-cooled monochrome CCD camera (AxioCam HRM, Carl Zeiss MicroImaging). The microscope was enclosed in a live cell incubator to maintain the experimental environment at 37°C and 5% CO_2. Images were analyzed with a custom-developed MATLAB program to calculate the deviation of the post centroid from its ideal position determined by the free and undeflected posts, which was then converted to the horizontal traction force by multiplying the nominal spring constant K calculated from the FEA simulations.

RESULTS

PDMS micropost arrays and micropatterned flat PDMS surfaces

Using microfabrication and replica molding (see **Methods**), we generated two sets of hexagonally spaced 1:10 PDMS micropost arrays, with each set of different post diameters and both covering a broad range of substrate rigidities by independently modulating their post heights. The first set of PDMS micropost arrays had a post diameter D of 0.8 μm, a post center-to-center (c.t.c.) distance S of 2 μm, and post heights L ranging from 0.42 μm to 13.45 μm (Fig. 1a&b). The other set of PDMS micropost arrays had a post diameter D of 1.83 μm, a post c.t.c. distance S of 4 μm, and post heights L ranging from 0.97 μm to 14.7 μm (Fig. 1c&d) [31]. For convenience, the PDMS micropost array with a post diameter of x μm and a post height of y μm was designated as 'micropost array $D(x)L(y)$'. Mechanical stiffness of the PDMS micropost array was characterized by its effective *Young*'s modulus E_{eff} (see **Methods**), which depended solely on the geometrical factors of the micropost array and the *Young*'s modulus E of PDMS (see discussion in **Introduction**) [32]. The PDMS micropost arrays in Fig. 1 span a more than 10,000-fold range of equivalent modulus E_{eff} from 0.1 kPa to 1,200 kPa, a range much broader than is currently achievable with natural or synthetic hydrogels [22, 23]. To study the synergistic and independent effects of substrate rigidity and adhesive ECM pattern on behaviors of mechanosensitive adherent cells, three different PDMS micropost arrays were deliberately selected from each of the two sets of the PDMS micropost arrays (Fig. 1e&f) and paired together based on their comparable effective moduli E_{eff}. The three chosen effective moduli E_{eff} (1 kPa or *soft* (D(0.8)L(6.23) *vs.* D(1.83)L(12.9)), 15 kPa or *medium* rigidity (D(0.8)L(2.48) *vs.* D(1.83)L(6.1)), and 1,200 kPa or *rigid* (D(0.8)L(0.42) *vs.* D(1.83)L(0.97)) covered a broad range of mechanical stiffness and were physiologically relevant to different human tissues where mechanics and forces have been proven important for their physiological and pathological functions [5, 21, 39]. We further applied microcontact stamp-off to pattern flat and featureless PDMS surfaces with distinct patterns of adhesive ECM islands (Fig. 2a) [36]. Patterns of ECM islands on the flat PDMS surfaces matched the top surfaces of the two sets of PDMS micropost arrays, enabling control studies of mechanosensitive cellular behaviors on flat PDMS surfaces (Fig. 2b&c). Uniformly coated flat PDMS surface was also generated to gauge the effect of available adhesive area on mechanosensitive cellular behaviors. Using

simple geometrical calculations, we further quantified adhesive properties, including the number of micropost (or adhesive island) per area and percentage of available adhesive area, for the PDMS micropost arrays and patterned flat PDMS surfaces (Figs. 1f&2d). We also modulated the ratio of the curing agent to base (either 1:10 or 1:30) for the PDMS prepolymer, to regulate bulk *Young*'s modulus *E* of the flat PDMS substrates (Fig. 2d).

Synergistic regulation of cell spreading and FA formation

We first used immunohistochemistry to examine independent effects of matrix rigidity and adhesive ECM pattern on cell spreading and FA formation for two different mechanosensitive mammalian cells, NIH/3T3 fibroblasts and human umbilical vein endothelial cells (HUVECs) (Fig. 3a). Both types of cells have previously been shown to respond to mechanical cues both *in vivo* and *in vitro* [40–42]. To examine their mechanosensitivity, both cells were sparsely plated on the three pairs of PDMS micropost arrays with different values of E_{eff}. Similar to our previous observations with human mesenchymal stem cells (hMSCs) [31, 35], both NIH/3T3 and HUVECs could respond to rigidity changes of the PDMS micropost array and exhibited marked differences in their degrees of attachment and spreading. Both cells plated on the soft PDMS micropost arrays (E_{eff} ~ 1 kPa; *D*(0.8)*L*(6.23) and *D*(1.83)*L*(12.9)) displayed a rounded or spindle-shaped morphology, poorly organized actin filaments, and small, punctuate adhesions. We also observed in some cases elongated adhesions bridging two or more PDMS microposts at the cell periphery for cells plated on the soft PDMS micropost arrays; this observation was more prominent for the *D*(0.8) micropost assays, which likely could be attributed to their shorter micropost c.t.c. distance and lower spring constant, facilitating FAs to bridge neighboring microposts. In contrast, cells cultured on the medium or rigid PDMS micropost arrays (E_{eff} ~ 15 kPa for *D*(0.8)*L*(2.48) and *D*(1.83)*L*(6.1) and E_{eff} ~ 1,200 kPa for *D*(0.8)*L*(0.42) and *D*(1.83)*L*(0.97)) spread to a large projected area and showed highly organized actin fiber networks and distinct and mature adhesions. Adhesion structures on the medium or rigid PDMS microposts were largely constrained by the surface geometry of the micropost top. Spatial organization of these adhesions closely mimicked the hexagonal arrangement of the PDMS micropost tops, especially at the cell periphery (Fig. 3a).

We further performed immunostaining assays for cells plated on functionalized flat PDMS surfaces. Figure 3b showed representative staining micrographs of NIH/3T3 cultured on 1:30 flat PDMS substrates (*E* ~ 800 kPa) coated with different ECM patterns. All cells were well spread out with prominent stress fibers and mature adhesions. NIH/3T3 cultured on uniformly coated flat PDMS surfaces spread out most, while cells on the flat PDMS surface coated with the *D*(1.83) pattern spread out least. Morphology of FAs and their spatial distribution and organization were significantly different for cells plated on flat PDMS surfaces coated with different ECM patterns. Specifically, NIH/3T3 on the uniformly coated flat PDMS surface could form large and elongated FAs (as long as 10 μm). However, on the flat PDMS substrates patterned with circular ECM islands, morphology of most FAs was constrained by the circular shape of the ECM islands. On the flat PDMS substrate coated with the *D*(0.8) pattern, more than 70% of FAs were isolated structures that were just as large as the adhesive ECM island, and the rest consisted of elongated adhesions bridging two or more neighboring adhesive islands. However, on the flat PDMS substrate coated with

the *D*(1.83) pattern, isolated FA structures tended to be smaller than the adhesive ECM islands, and elongated FAs bridging neighboring adhesive islands were very rare.

A detailed quantitative morphometric analysis of cell populations on cell spreading and FA formation revealed that, for both NIH/3T3 and HUVECs, population means of the cell spread area and total FA area per cell increased monotonically with E_{eff}, following roughly a power law dependence on E_{eff} with the scaling exponent decreasing with increasing E_{eff} (Fig. 4). It appeared that both cells were more sensitive to rigidity changes when 1 kPa < E_{eff} < 15 than when 15 kPa < E_{eff} < 1,200 kPa, as cell spread area and total FA area per cell increased more rapidly in the soft-to-medium rigidity range than in the mediumto-rigid one (Fig. 4a,b,d,e). This rigidity-dependent mechanosensitivity was also more apparent for HUVECs, as their cell spread area and total FA area per cell increased rapidly with E_{eff} in the soft-to-medium rigidity range and then started to level off in the medium-to-rigid range.

Adhesive ECM patterns of the PDMS micropost array could also affect rigidity-dependent cell spreading and FA formation. We observed that in Fig. 4, cells plated on the *D*(0.8) micropost arrays tended to exhibit greater cell spread area and total FA area per cell as compared to the ones on the *D*(1.83) arrays. Specifically, we observed that NIH/3T3 didn't show significant difference in cell spreading and FA formation when plated on the two soft PDMS micropost arrays (*D*(0.8)*L*(6.23) *vs.* *D*(1.83)*L*(12.9)) (Fig. 4a&b). However, as E_{eff} increased, influence of the adhesive ECM pattern on cell morphology became significant. For NIH/3T3, when compared with *D*(1.83) micropost arrays, *D*(0.8) arrays could induce greater population means of the cell spread area and FA area per cell by 46.3% and 35.9%, respectively, on the medium rigid micropost arrays (*D*(0.8)*L*(2.48) *vs.* *D*(1.83)*L*(6.1)), and 41.3% and 35.8%, respectively, on the rigid ones (*D*(0.8)*L*(0.42) *vs.* *D*(1.83)*L*(0.97)). For HUVECs, significant differences in cell spreading and FA formation were observed for cells plated on *D*(0.8) *vs.* *D*(1.83) micropost arrays for the entire rigidity range examined (Fig. 4d&e). We observed increases of population means of cell spread area and FA area per cell for HUVECs by 27.8% and 25.4%, respectively, on the soft micropost arrays (*D*(0.8)*L*(6.23) *vs.* *D*(1.83)*L*(12.9)), by 44.0% and 19.2%, respectively, on the medium rigid ones (*D*(0.8)*L*(2.48) *vs.* *D*(1.83)*L*(6.1)), and by 15.5% and 19.8 %, respectively, on the rigid ones (*D*(0.8)*L*(0.42) *vs.* *D*(1.83)*L*(0.97)).

Noticing that population means of cell spread area and total FA area per cell for both NIH/3T3 and HUVECs followed similar power law dependences on E_{eff}, we further performed single-cell correlative studies by plotting single-cell data of the total FA area per cell against cell spread area for both cell types. Figure 4c&f showed that all the single-cell data of the total FA area per cell collapsed and followed a single trend against cell spread area, regardless of substrate rigidity and adhesive ECM pattern.

Using immunostaining micrographs in Fig. 3b, we further performed a morphometric analysis for NIH/3T3 cells plated on flat PDMS surfaces coated with different ECM patterns. Figure 5a&b showed that for NIH/3T3, regulations of cell spreading and FA formation by substrate rigidity and adhesive ECM patterns were similar between flat PDMS surfaces and PDMS micropost arrays. Specifically, on flat PDMS surfaces with different ECM patterns, cell spread area and total FA area per cell would increase with the *Young*'s

modulus *E* of the PDMS substrate. Consistent with the results obtained from the PDMS micropost arrays, the *D*(0.8) adhesive pattern on flat PDMS surfaces tended to induce greater cell spreading and FA formation as compared to the *D*(1.83) pattern. We further performed a correlative study for single-cell data of cell spread area and total FA area per cell for NIH/3T3. On both 1:30 and 1:10 flat PDMS substrates, cell spread area and total FA area per cell were strongly positively correlated, regardless of the specific adhesive ECM pattern (Fig. 5c&d). All together, our morphometric analysis in Fig. 4&5 suggested that mechanoresponsive behaviors of adherent cells might be mediated by both matrix rigidity and adhesive ECM pattern, and their synergistic regulation of cell-ECM interactions could be cell-type specific and depend on the specific rigidity range of the substrate the cells adhere to. Our comparative and correlative studies in Fig. 4&5 also strongly indicated that cell shape and FA structures were tightly coupled mechanosensitive systems involved in transducing physical signals in cell microenvironment into intracellular responses, and it was highly plausible that cell shape could provide a global physical parameter to control cell-ECM interactions to regulate the mechanosensitive behaviors of adherent cells through mediating their adhesion formation and signaling [3, 19].

Synergistic regulation of cytoskeletal contractility

Cell-ECM interactions are closely regulated by intracellular cytoskeletal contractility, which directly mediates FA formation and signaling to control downstream cellular functions [1–3, 43]. Using the PDMS microposts as traction force sensors [32, 34], we performed live-cell imaging to further quantify independent effects of matrix rigidity and adhesive ECM pattern on cytoskeletal contractility of NIH/3T3 and HUVECs (Fig. 6). For these contractility measurements, we used PDMS micropost arrays with 1 kPa < E_{eff} < 15 kPa (Fig. 1f), with which a custom-developed MATLAB program could accurately determine traction forces exerted on adhesions on the PDMS micropost tops by measuring their deflections [35] (Fig. 6a&g). Our quantitative analysis of contractility in Fig. 6b&h revealed that for both NIH/3T3 and HUVECs, cellular traction force increased monotonically with E_{eff} for 1 kPa < E_{eff} <15 kPa. Effect of adhesive ECM pattern on cell contractility appeared to be cell-type specific. For NIH/3T3, when E_{eff} < 5 kPa, no significant difference in traction force was observed between the *D*(0.8) and *D*(1.83) micropost arrays. As E_{eff} > 5 kPa, it appeared that the *D*(0.8) micropost arrays could elicit stronger traction forces than the *D*(1.83) ones. For HUVECs, the traction force-E_{eff} curves for the *D*(0.8) and *D*(1.83) micropost arrays appeared largely overlapped with each other, suggesting that rigidity-dependent contractility of HUVECs was not sensitive to the adhesive ECM patterns examined in this study, at least for 1 kPa < E_{eff} < 15 kPa. We further performed correlative studies of single-cell data of traction force and cell spread area. Our data in Fig. 6d&e and Fig. 6j&k showed strong linear correlations between traction force and cell spread area, for both NIH/3T3 and HUVECs and under different ECM rigidity and adhesive ECM pattern conditions. Slopes of the linear correlations between traction force and cell spread area increased with E_{eff}. For NIH/3T3, the slopes of these linear fits were greater for the *D*(0.8) micropost arrays than the *D*(1.83) ones for E_{eff} > 5 kPa (Fig. 6f). This observation was reversed for HUVECs, as slopes of their linear fits were greater for the *D*(1.83) micropost arrays than the *D*(0.8) ones (Fig. 6l).

Synergistic regulation of cell proliferation

We examined synergistic regulation of cell proliferation by matrix rigidity and adhesive ECM pattern using the standard EdU assay. NIH/3T3 and HUVECs were sparsely plated on both PDMS micropost arrays and flat PDMS surfaces coated with different ECM patterns, and then assayed for their proliferation. As shown in Fig. 7a&b, for both cells, their proliferation rate would increase rapidly with E_{eff} and then gradually level off with an asymptotic plateau. A strong influence of adhesive ECM pattern on cell proliferation was observed, especially for E_{eff} < 10 kPa (Fig. 7a&b). For E_{eff} < 10 kPa, cell proliferation rates for both NIH/3T3 and HUVECs were significantly higher on the *D*(0.8) micropost arrays than those on the *D*(1.83) ones. Effect of adhesive ECM pattern on cell proliferation was gradually diminished as E_{eff} increased above certain threshold values (about 1,000 kPa and 200 kPa for NIH/3T3 and HUVECs, respectively). Adhesive ECM patterns also had a strong influence on cell proliferation for both 1:30 and 1:10 flat PDMS surfaces (Fig. 7c), which had relatively large *Young*'s modulus *E* (*E*(1:30 PDMS) ~ 800 kPa and *E*(1:10 PDMS) ~ 2.5 MPa). For both 1:30 and 1:10 PDMS, proliferation rate of NIH/3T3 was the greatest on the uniformly coated flat PDMS surface and then became less on the PDMS surface coated with the *D*(0.8) pattern. Proliferation rate of NIH/3T3 was the least on the flat PDMS surfaces coated with the *D*(1.83) pattern.

DISCUSSION

In this work, we used microfabrication and replica-molding to generate a broad range of PDMS micropost arrays with different post diameters and heights. Using these PDMS micropost arrays together with flat and featureless PDMS surfaces coated with different ECM patterns, we took a comprehensive and systematic approach to study the independent and synergistic effects of substrate rigidity and adhesive ECM pattern on mechanoresponsive cellular behaviors for both NIH/3T3 and HUVECs. We showed that both substrate rigidity and adhesive ECM pattern could regulate mechanoresponsive cellular behaviors, including cell spreading, FA formation, cytoskeletal contractility, and proliferation.

Specifically, our data suggested that within the rigidity range examined in this work (1 kPa < E_{eff} < 1,200 kPa), cell spread area, FA formation, cytoskeletal contractility, and cell proliferation rate for both NIH/3T3 and HUVECs increased monotonically with substrate rigidity E_{eff}. Such rigidity-dependent mechanoresponsive cellular behaviors were most apparent with 1 kPa < E_{eff} < 10 kPa, consistent with the fact that vascular and embryo tissues have their intrinsic mechanical rigidity in the range of 1 kPa to 10 kPa [21, 39]. When E_{eff} > 10 kPa, mechanoresponsive cellular behaviors in both cells could gradually lose their sensitivity to rigidity changes. This observation was strongly evident in the mechanoresponsive cell proliferation, as both cells would increase their proliferation rate rapidly with E_{eff} when E_{eff} < 10 kPa and then level off quickly with different asymptotic levels.

Our results further showed a strong influence of adhesive ECM pattern on rigidity-mediated cell morphology, FA formation, cytoskeletal contractility, and proliferation. Compared with the *D*(0.8) micropost arrays, the *D*(1.83) ones induced less cell spreading, FA formation, and

cell proliferation. Effect of adhesive ECM pattern on rigidity-mediated cell morphology, FA formation, and proliferation rate was further confirmed with flat PDMS surfaces coated with different ECM patterns. Combined together with the observation that both cells could adapt to form FA structures bridging adjacent adhesive islands, our study suggested that the available number of adhesion sites per area (which was 0.288 μm^{-2} for the *D*(0.8) micropost arrays and 0.072 μm^{-2} for the *D*(1.83) ones; Fig. 2d) might play a more influential role in regulating cell morphology, FA formation, and proliferation than the percentage of available adhesive area (which was 19% for the *D*(1.83) micropost arrays and 14.5% for the *D*(0.8) ones; Fig. 2d). The effect of adhesive ECM pattern on rigidity-dependent cell contractility showed some differences between NIH/3T3 and HUVECs, which was especially true for the ratio of total cell contractility per cell to cell spread area, as their dependence on E_{eff} was completely reversed between the *D*(0.8) and *D*(1.83) micropost arrays (Fig. 6f&l).

Our morphometric analysis of cell populations showed a strong positive correlation between FA formation and cell spread area for both NIH/3T3 and HUVECs, regardless of micropost rigidity and adhesive ECM pattern (Fig. 4c&f and Fig. 5c&d), consistent with our previous observations for hMSCs [31]. We also observed a strong correlation between traction force and cell spreading, with a substantially smaller independent effect of micropost rigidity on traction force. Together, these results suggested that cell area and FA formation might be tightly coupled cellular biomechanical systems involved in mechanosensing, and the simple phenomenological laws describing their correlations appeared to be both universal and primitive, highlighting the important role of cell shape change involved in the complex control loop governing the cellular mechanosensing mechanism. How substrate rigidity regulates cell shape is not yet understood and could likely involve unknown physical and biomechanical mechanisms. Given that substrate rigidity mediates integrin and FA signaling [1–3, 44], it is reasonable to speculate involvement of rigidity mediated integrin and FA activities in regulating cell shape change, and such cell shape change could feed back to regulate the global FA formation and signaling. Investigations of such mechanistic questions are clearly out of the scope of this current study, but nonetheless, we believe the PDMS micropost arrays reported in this work could provide an ideal and efficient test bed for such detailed future investigations requiring completely decoupling of matrix rigidity and adhesive ECM pattern.

CONCLUSIONS

In this work, we used microfabrication and replica molding to successfully generate a library of PDMS micropost arrays with a broad range of structural geometries. Compared with conventional natural or synthetic hydrogels used for studying cell-ECM interactions, our PDMS micropost arrays offered the advantage of independent regulations and complete decoupling of different substrate surface properties, including ligand density and adhesive ECM pattern and bulk and nanoscale mechanics of the substrate materials. We applied these PDMS micropost arrays to systematically study the synergistic and independent effects of matrix rigidity and adhesive ECM pattern on mechanoresponsive cellular behaviors, including cell spreading, FA formation, cytoskeletal contractility, and proliferation. Our results demonstrated a close interplay of matrix rigidity and adhesive ECM pattern in regulating mechanoresponsive cellular behaviors in a cell type-specific manner. Correlative

morphometric studies further revealed strong functional links between FA formation, cell morphology, and cytoskeletal contractility during the intriguing mechanosensory processes. Our investigations not only suggested the important applications of our PDMS micropost arrays in investigating mechano-sensing and –transduction processes and biointerfacial phenomena, but also provided the basis for future studies to unravel integrated cellular responses to complex biomechanical stimuli and to design synthetic biomaterials for tissue engineering and regenerative medicine.

Acknowledgments

We acknowledge financial support from the National Science Foundation (NSF CMMI 1129611) and the department of Mechanical Engineering at the University of Michigan, Ann Arbor. We thank P. Mao for his assistance in microfabrication and taking scanning electron microscopy images. We acknowledge valuable comments and suggestions on the manuscript by group members of the Integrated Biosystems and Biomechanics Laboratory (R. Lam, W. Chen, Y. Sun, and J. Mann). We thank M. Yang and C. Chen for sharing with us their MATLAB program to quantify cellular traction forces. The Massachusetts Institute Technology (M.I.T.) Microsystems Technology Laboratories (MTL) is acknowledged for support in microfabrication.

REFERENCES

1. Hoffman BD, Grashoff C, Schwartz MA. Dynamic molecular processes mediate cellular mechanotransduction. Nature. 2011; 475(7356):316–323. [PubMed: 21776077]
2. Geiger B, Spatz JP, Bershadsky AD. Environmental sensing through focal adhesions. Nat Rev Mol Cell Biol. 2009; 10(1):21–33. [PubMed: 19197329]
3. Chen CS. Mechanotransduction - a field pulling together? J Cell Sci. 2008; 121(20):3285–3292. [PubMed: 18843115]
4. Vogel V, Sheetz M. Local force and geometry sensing regulate cell functions. Nat Rev Mol Cell Biol. 2006; 7(4):265–275. [PubMed: 16607289]
5. Discher DE, Janmey P, Wang YL. Tissue cells feel and respond to the stiffness of their substrate. Science. 2005; 310:1139–1143. [PubMed: 16293750]
6. Connelly JT, Gautrot JE, Trappmann B, Tan DWM, Donati G, Huck WTS, et al. Actin and serum response factor transduce physical cues from the microenvironment to regulate epidermal stem cell fate decisions. Nat Cell Biol. 2010; 12(7) 711-U177.
7. McBeath R, Pirone DM, Nelson CM, Bhadriraju K, Chen CS. Cell shape, cytoskeletal tension, and RhoA regulate stem cell lineage commitment. Dev Cell. 2004; 6:483–495. [PubMed: 15068789]
8. Chen CS, Mrksich M, Huang S, Whitesides GM, Ingber DE. Geometric control of cell life and death. Science. 1997; 276:1425–1428. [PubMed: 9162012]
9. Huebsch N, Arany PR, Mao AS, Shvartsman D, Ali OA, Bencherif SA, et al. Harnessing traction-mediated manipulation of the cell/matrix interface to control stem-cell fate. Nat Mater. 2010; 9(6): 518–526. [PubMed: 20418863]
10. Gilbert PM, Havenstrite KL, Magnusson KEG, Sacco A, Leonardi NA, Kraft P, et al. Substrate elasticity regulates skeletal muscle stem cell selfrenewal in culture. Science. 2010; 329:1078–81. [PubMed: 20647425]
11. Mammoto A, Connor KM, Mammoto T, Yung CW, Huh D, Aderman CM, et al. A mechanosensitive transcriptional mechanism that controls angiogenesis. Nature. 2009; 457:1103–1108. [PubMed: 19242469]
12. Levental KR, Yu H, Kass L, Lakins JN, Egeblad M, Erler JT, et al. Matrix crosslinking forces tumor progression by enhancing integrin signaling. Cell. 2009; 139(5):891–906. [PubMed: 19931152]
13. Isenberg BC, DiMilla PA, Walker M, Kim S, Wong JY. Vascular smooth muscle cell durotaxis depends on substrate stiffness gradient strength. Biophys J. 2009; 97(5):1313–1322. [PubMed: 19720019]

14. Engler AJ, Sen S, Sweeney HL, Discher DE. Matrix elasticity directs stem cell lineage specification. Cell. 2006; 126:677–689. [PubMed: 16923388]
15. Paszek MJ, Zahir N, Johnson KR, Lakins JN, Rozenberg GI, Gefen A, et al. Tensional homeostasis and the malignant phenotype. Cancer Cell. 2005; 8(3):241–254. [PubMed: 16169468]
16. Dalby MJ, Gadegaard N, Tare R, Andar A, Riehle MO, Herzyk P, et al. The control of human mesenchymal cell differentiation using nanoscale symmetry and disorder. Nat mater. 2007; 6(12): 997–1003. [PubMed: 17891143]
17. Yim EK, Reano RM, Pang SW, Yee AF, Chen CS, Leong KW. Nanopattern-induced changes in morphology and motility of smooth muscle cells. Biomaterials. 2005; 26(26):5405–5413. [PubMed: 15814139]
18. Curtis A, Wilkinson C. Topographical control of cells. Biomaterials. 1997; 18(24):1573–1583. [PubMed: 9613804]
19. Shen C, Fu J, Chen C. Patterning cell and tissue function. Cell Mol Bioeng. 2008; 1(1):15–23.
20. Peyton S, Ghajar C, Khatiwala C, Putnam A. The emergence of ECM mechanics and cytoskeletal tension as important regulators of cell function. Cell Biochem Biophys. 2007; 47(2):300–320. [PubMed: 17652777]
21. Janmey PA, McCulloch CA. Cell mechanics: integrating cell responses to mechanical stimuli. Annu Rev Biomed Eng. 2007; 9(1):1–34. [PubMed: 17461730]
22. Georges PC, Janmey PA. Cell type-specific response to growth on soft materials. J Appl Physiol. 2005; 98(4):1547–1553. [PubMed: 15772065]
23. Wong JY, Leach JB, Brown XQ. Balance of chemistry, topography, and mechanics at the cell-biomaterial interface: Issues and challenges for assessing the role of substrate mechanics on cell response. Surf Sci. 2004; 570(1–2):119–133.
24. Lo CM, Wang HB, Dembo M, Wang YL. Cell movement is guided by the rigidity of the substrate. Biophys J. 2000; 79(1):144–152. [PubMed: 10866943]
25. Pelham RJ, Wang YL. Cell locomotion and focal adhesions are regulated by substrate flexibility. Proc Natl Acad Sci U S A. 1997; 94(25):13661–13665. [PubMed: 9391082]
26. Mei Y, Saha K, Bogatyrev SR, Yang J, Hook AL, Kalcioglu ZI, et al. Combinatorial development of biomaterials for clonal growth of human pluripotent stem cells. Nat Mater. 2010; 9(9):768–778. [PubMed: 20729850]
27. Keselowsky BG, Collard DM, García AJ. Integrin binding specificity regulates biomaterial surface chemistry effects on cell differentiation. Proc Natl Acad Sci U S A. 2005; 102(17):5953–5957. [PubMed: 15827122]
28. Houseman BT, Mrksich M. The microenvironment of immobilized Arg-Gly-Asp peptides is an important determinant of cell adhesion. Biomaterials. 2001; 22(9):943–955. [PubMed: 11311013]
29. Lutolf MP, Hubbell JA. Synthetic biomaterials as instructive extracellular microenvironments for morphogenesis in tissue engineering. Nat Biotechnol. 2005; 23(1):47–55. [PubMed: 15637621]
30. Vunjak-Novakovic G, Scadden DT. Biomimetic platforms for human stem cell research. Cell Stem Cell. 2011; 8(3):252–261. [PubMed: 21362565]
31. Fu J, Wang YK, Yang MT, Desai RA, Yu X, Liu Z, et al. Mechanical regulation of cell function using geometrically modulated elastomeric substrates. Nature Methods. 2010; 7:733–736. [PubMed: 20676108]
32. Saez A, Buguin A, Silberzan P, Ladoux B. Is the mechanical activity of epithelial cells controlled by deformations or forces? Biophys J. 2005; 89(6):L52–L54. [PubMed: 16214867]
33. du Roure O. Force mapping in epithelial cell migration. Proc Natl Acad Sci U S A. 2005; 102:2390–2395. [PubMed: 15695588]
34. Tan JL, Tien J, Pirone DM, Gray DS, Bhadriraju K, Chen CS. Cells lying on a bed of microneedles: An approach to isolate mechanical force. Proc Natl Acad Sci U S A. 2003; 100(4): 1484–1489. [PubMed: 12552122]
35. Yang MT, Fu J, Wang YK, Desai RA, Chen CS. Assaying stem cell mechanobiology on microfabricated elastomeric substrates with geometrically modulated rigidity. Nat Protoc. 2011; 6:187–213. [PubMed: 21293460]

36. Desai RA, Khan MK, Gopal SB, Chen CS. Subcellular spatial segregation of integrin subtypes by patterned multicomponent surfaces. Integr Biol(Camb). 2011; 3(5):560–567. [PubMed: 21298148]

37. Pirone DM, Liu WF, Ruiz SA, Gao L, Raghavan S, Lemmon CA, et al. An inhibitory role for FAK in regulating proliferation: a link between limited adhesion and RhoA-ROCK signaling. J Cell Biol. 2006; 174(2):277–288. [PubMed: 16847103]

38. Yang MT, Sniadecki NJ, Chen CS. Geometric Considerations of Micro- to Nanoscale Elastomeric Post Arrays to Study Cellular Traction Forces. Adv mater. 2007; 19(20):3119–3123.

39. Bao G, Suresh S. Cell and molecular mechanics of biological materials. Nat Mater. 2003; 2(11): 715–725. [PubMed: 14593396]

40. Hahn C, Schwartz MA. Mechanotransduction in vascular physiology and atherogenesis. Nat Rev Mol Cell Biol. 2009; 10(1):53–62. [PubMed: 19197332]

41. Chien S. Mechanotransduction and endothelial cell homeostasis: the wisdom of the cell. Am J Physiol Heart Circ Physiol. 2007; 292(3):H1209–H1224. [PubMed: 17098825]

42. Ingber DE. Mechanobiology and diseases of mechanotransduction. Ann Med. 2003; 35(8):564–577. [PubMed: 14708967]

43. Wozniak MA, Chen CS. Mechanotransduction in development: a growing role for contractility. Nat Rev Mol Cell Biol. 2009; 10(1):34–43. [PubMed: 19197330]

44. Schwartz MA, DeSimone DW. Cell adhesion receptors in mechanotransduction. Current Opin Cell Biol. 2008; 20(5):551–556.

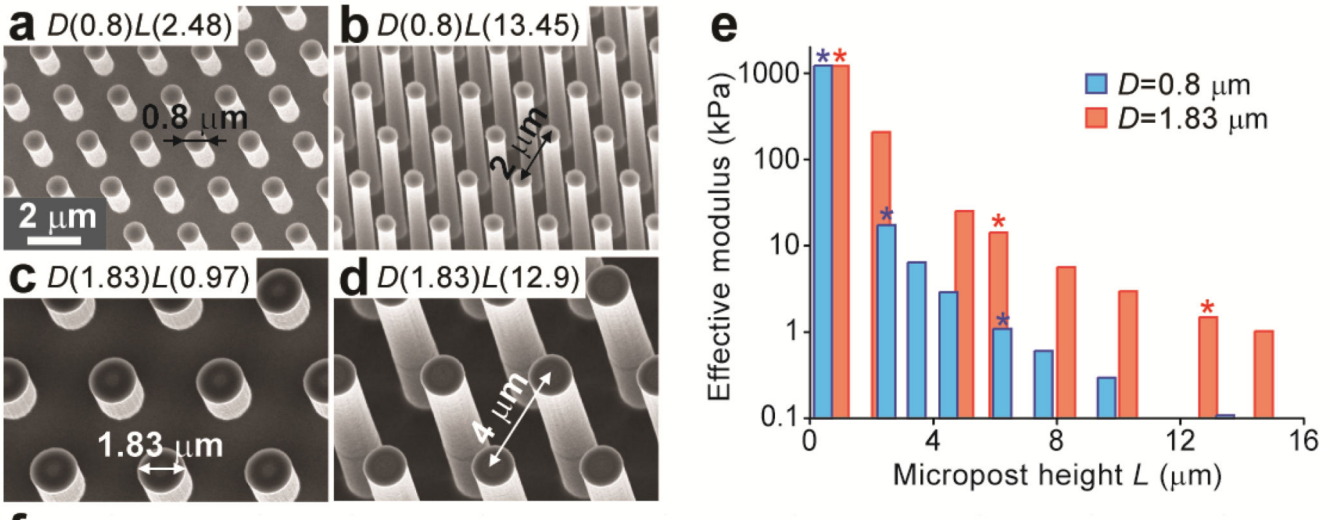

f

Array designation		Tip diam. D (μm)	Center-to-center dist. S (μm)	# of post per area (μm^{-2})	Available adhesive area (%)	Post height L (μm)	Post rigidity K (nN/μm)	Effective modulus E_{eff} (kPa)
D(0.8)	D(0.8)L(0.42)*	0.8	2	0.288	14.5	0.42	688.4	1232.6
	D(0.8)L(2.48)*					2.48	9.7	17.4
	D(0.8)L(3.46)					3.46	3.6	6.4
	D(0.8)L(4.49)					4.49	1.6	2.9
	D(0.8)L(6.23)*					6.23	0.6	1.1
D(1.83)	D(1.83)L(0.97)*	1.83	4	0.072	19	0.97	1556.7	1218.5
	D(1.83)L(6.1)*					6.1	18.2	14.2
	D(1.83)L(8.3)					8.3	7.2	5.6
	D(1.83)L(10.3)					10.3	3.8	3.0
	D(1.83)L(12.9)*					12.9	1.9	1.5

Figure 1.

Microfabricated PDMS micropost arrays to engineer substrate rigidity and adhesive ECM patterns. (**a–d**) Representative scanning electron microscopy (SEM) images of hexagonally arranged silicon micropost masters. **a** and **b** show two masters sharing the same post diameter D of 0.8 μm and center-to-center (c.t.c.) distance S of 2 μm, while **c** and **d** are two masters with the same post diameter D of 1.83 μm and c.t.c distance S of 4 μm. (**e**) Dependence of effective modulus E_{eff} of the PDMS micropost array on the post height L (*blue*: D=0.8 μm, S=2 μm; *red*: D=1.83 μm, S=4 μm). (**f**) Table summarizing different geometrical factors and their associated mechanical and adhesive properties of the PDMS micropost arrays. Asterisks (*) in **e** and **f** mark the chosen PDMS micropost arrays with similar E_{eff} for comparative morphological studies in this work.

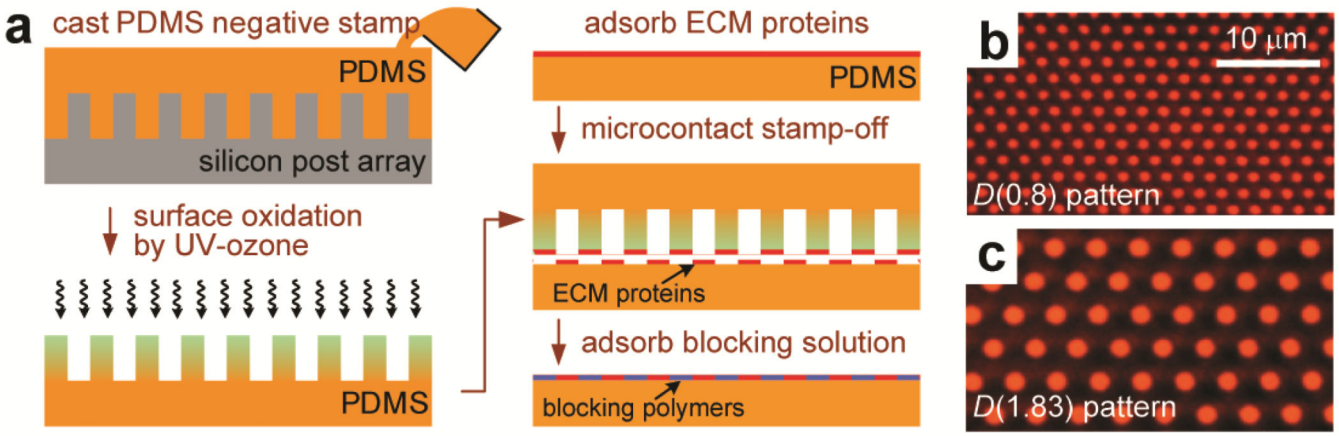

d

Substrate designation	ECM island diameter D (μm)	Center-to-center dist. S (μm)	# of island per area (μm^{-2})	Available adhesive area (%)	Young's Modulus (kPa)	
					1:30 PDMS	1:10 PDMS
Uniform	N/A	N/A	N/A	100	~800	~2500
D(0.8) pattern	0.8	2	0.288	14.5		
D(1.83) pattern	1.83	4	0.072	19		

Figure 2.

Flat PDMS substrates patterned with adhesive ECM islands using microcontact stamp-off. (**a**) Schematic of microcontact stamp-off to pattern flat PDMS surfaces with adhesive ECM islands. (**b&c**) Fluorescence images of flat PDMS surfaces coated with arrays of hexagonally arranged circular ECM islands using microcontact stamp-off (**b**: D=0.8 μm, S=2 μm; **c**: D=1.83 μm, S=4 μm). Bovine serum albumin (BSA) conjugated with Alexa Fluor-555 was used for visualization of patterned proteins. Note the lack of fluorescence signal outside of the patterned circles, indicting complete protein removal using microcontact stamp-off. (**d**) Table summarizing flat PDMS substrates coated with different ECM patterns as controls for the comparative studies. 'Uniform' PDMS surfaces were coated uniformly with ECM proteins by natural adsorption. 'D(0.8) pattern' PDMS substrates were coated with circular ECM islands with D=0.8 μm and S=2 μm, while 'D(1.83) pattern' PDMS substrates were coated with circular ECM islands with D=1.83 μm and S=4 μm. PDMS with different curing agent:base ratios (1:30 and 1:10; w/w) were used to regulate substrate rigidity.

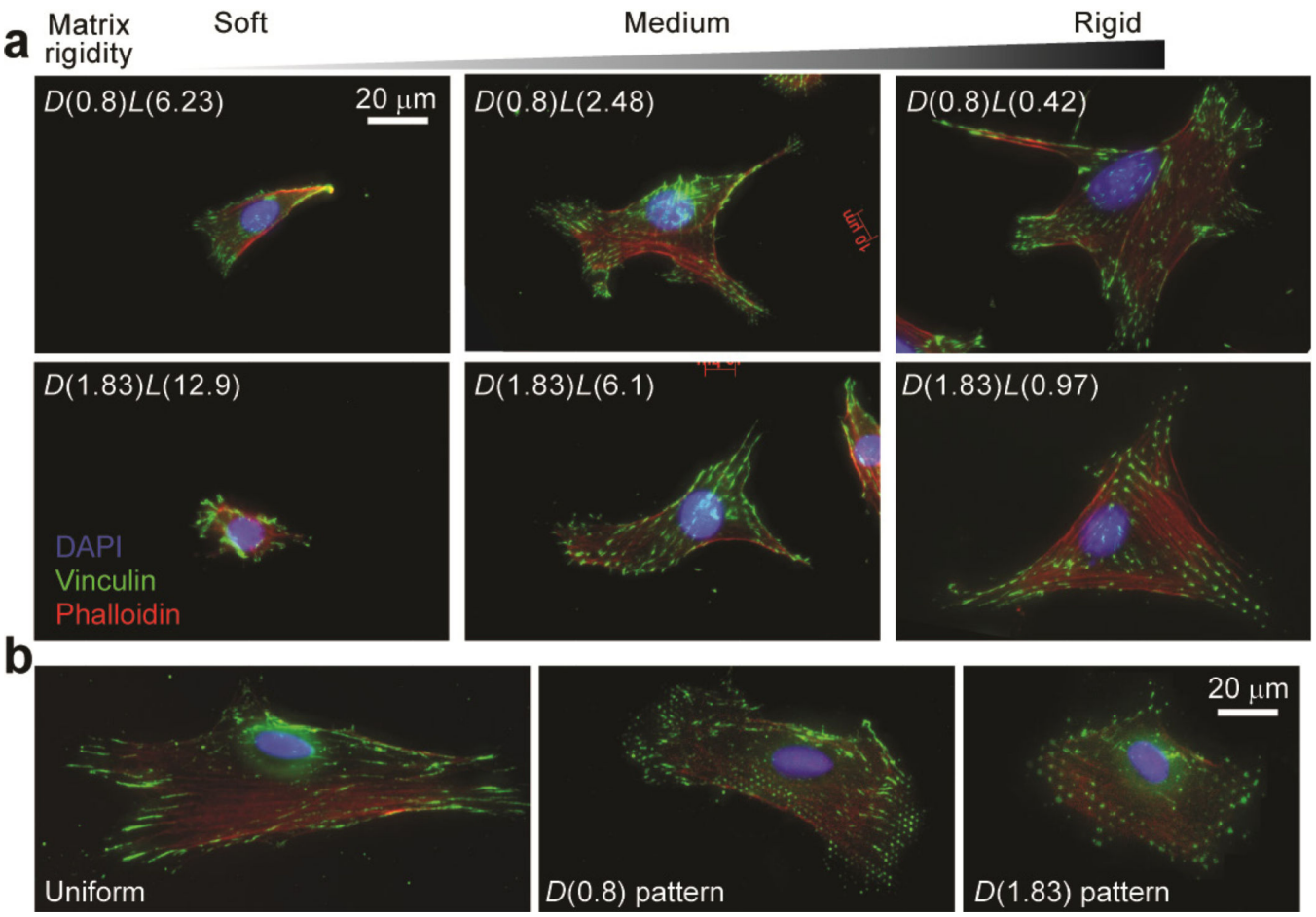

Figure 3.

Representative immunofluorescence images of single NIH/3T3 cells plated on different PDMS-based substrates. Cells were grown overnight in the complete growth medium prior to fixation, and were stained with DAPI, fluorophore-labeled phalloidin and anti-vinculin to visualize nuclei, actin filaments, and FAs, respectively. (**a**) Single NIH/3T3 cells plated on the PDMS micropost arrays of different geometries and rigidities as indicated. (**b**) Single NIH/3T3 cells plated on flat PDMS surfaces coated with different ECM patterns as indicated.

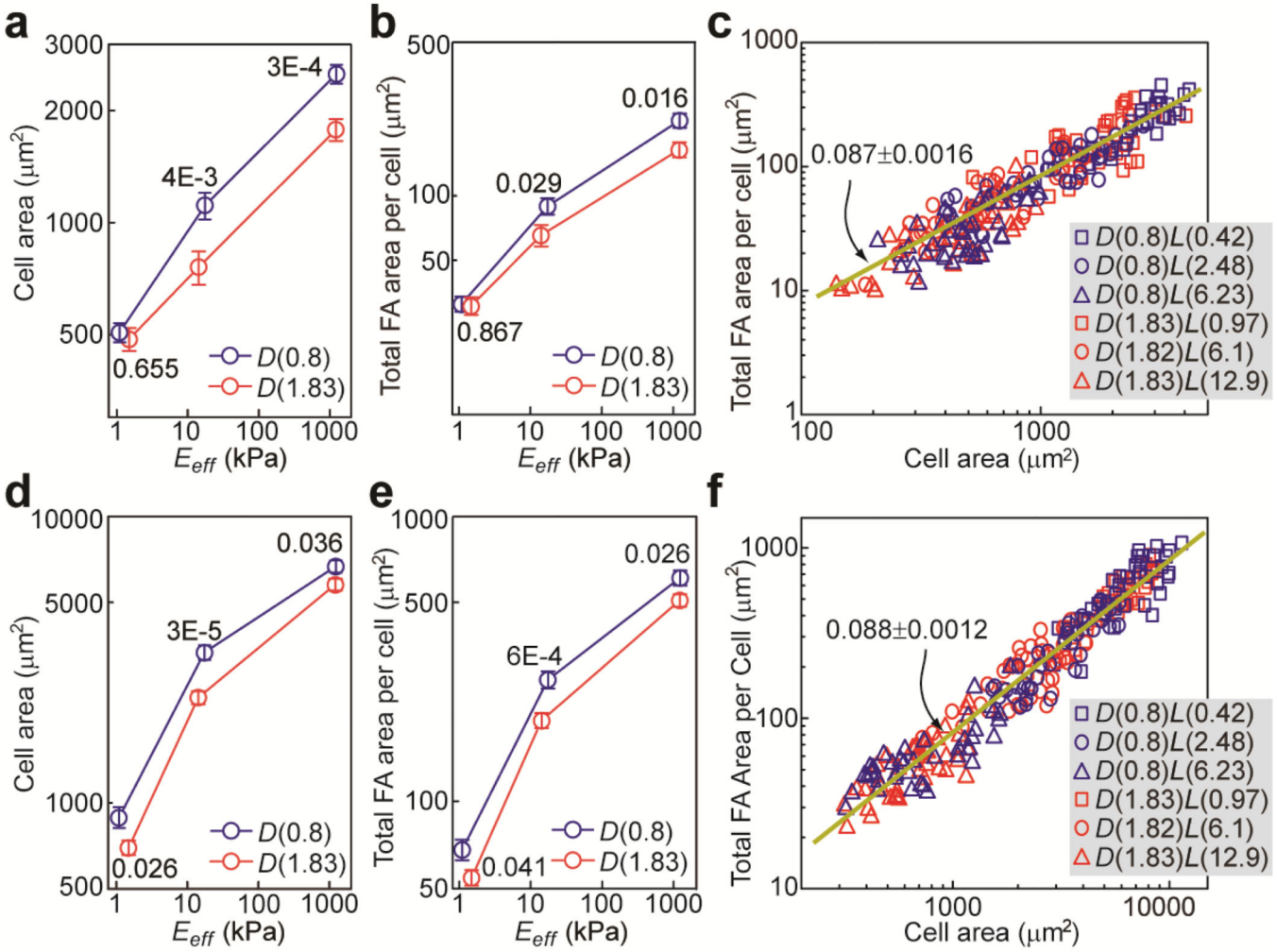

Figure 4.

Quantitative and correlative analysis of cell morphology and FA formation for NIH/3T3 (**a–c**) and HUVECs (**d–f**) plated on the PDMS micropost arrays of different geometries and rigidities. Cell spread area (**a, d**) and total FA area per cell (**b, e**) were plotted against effective modulus E_{eff} of the PDMS micropost array. Error bars represent the standard error of mean (s.e.m), and $n = 40$ for each condition. *P*-values calculated using the paired student's *t*-test were indicated for statistically significant differences. In **c** & **f**, total FA area per cell was plotted against cell spread area. Each data point in **c** & **f** represents an individual cell, and $n = 240$. Data were collected from six different PDMS micropost arrays as indicated. Data trends in **c** & **f** were plotted using linear least square fitting (dark yellow lines), with the slope values ± s.e.m. indicated.

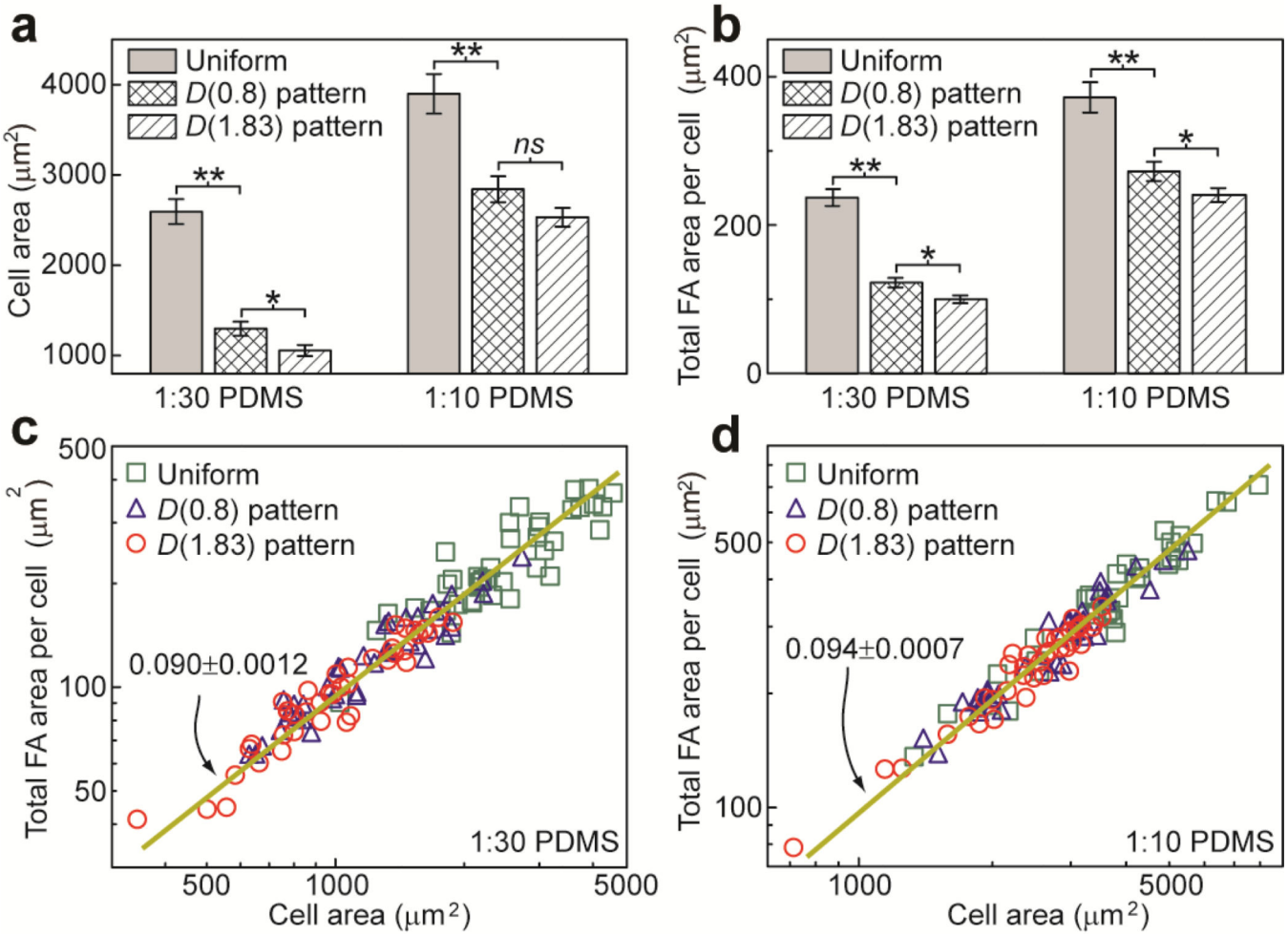

Figure 5.

Quantitative and correlative analysis of NIH/3T3 cells plated on 1:10 and 1:30 flat PDMS substrates coated with different adhesive ECM patterns. (**a&b**) Column plots of cell spread area (**a**) and total FA area per cell (**b**) as a function of PDMS substrate rigidity and adhesive ECM pattern as indicated. Error bars represent ± s.e.m. *P*-values calculated using the paired student's *t*-test were indicated for statistically significant differences ($P > 0.05$ (not significant, or *ns*), $P < 0.05$ (*), and $P < 0.005$ (**)). (**c&d**) Total FA area per cell versus cell spread area plotted for 1:30 (**c**) and 1:10 (**d**) flat PDMS substrates coated with different ECM patterns as indicated. Data trends were plotted using linear least square fitting (dark yellow lines), with the slope values ± s.e.m indicated.

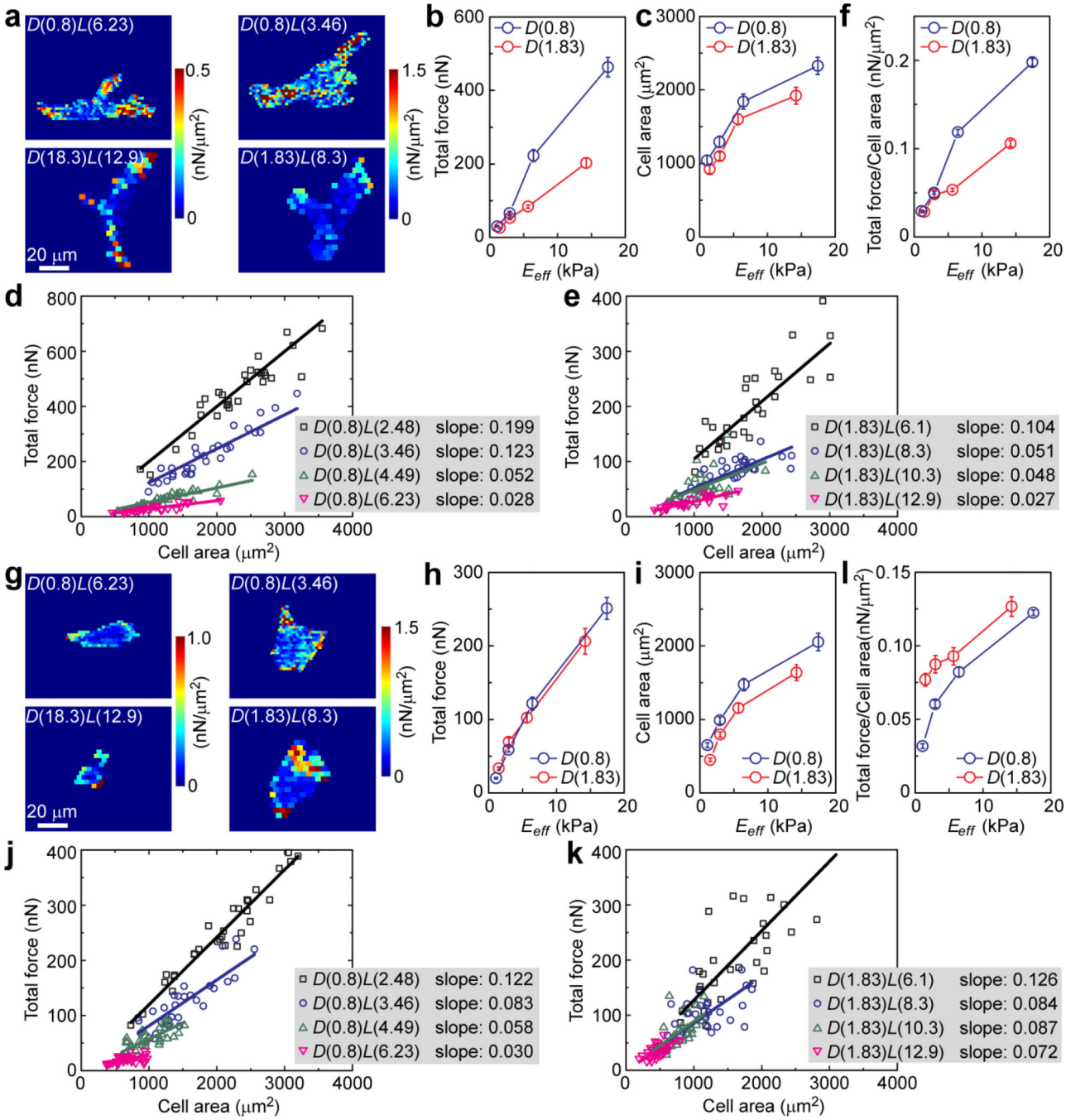

Figure 6.

Quantitative and correlative analysis of intracellular cytoskeletal contractility for NIH/3T3 (**a–f**) and HUVECs (**g–l**) plated on the PDMS micropost arrays of different geometries and rigidities. **a** and **g** are representative colorimetric maps of contractile stress (defined here as the ratio of traction force to micropost top surface area) for single NIH/3T3 (**a**) and HUVECs (**g**) plated on the PDMS micropost arrays of different geometries but with comparable rigidities as indicated. Total traction force (**b, h**), cell spread area (**c, i**), and total traction force per cell area (**f, l**) were plotted against E_{eff}. Error bars represent the s.e.m., and

n = 30 for each condition. Single cell data of total traction force was plotted against cell spread area for micropost array set D(0.8) (**d, j**) and set D(1.83) (**e, k**). Each data point in **d, e, j** and **k** represents an individual cell, and data trends were plotted using linear least square fitting with the slopes indicated.

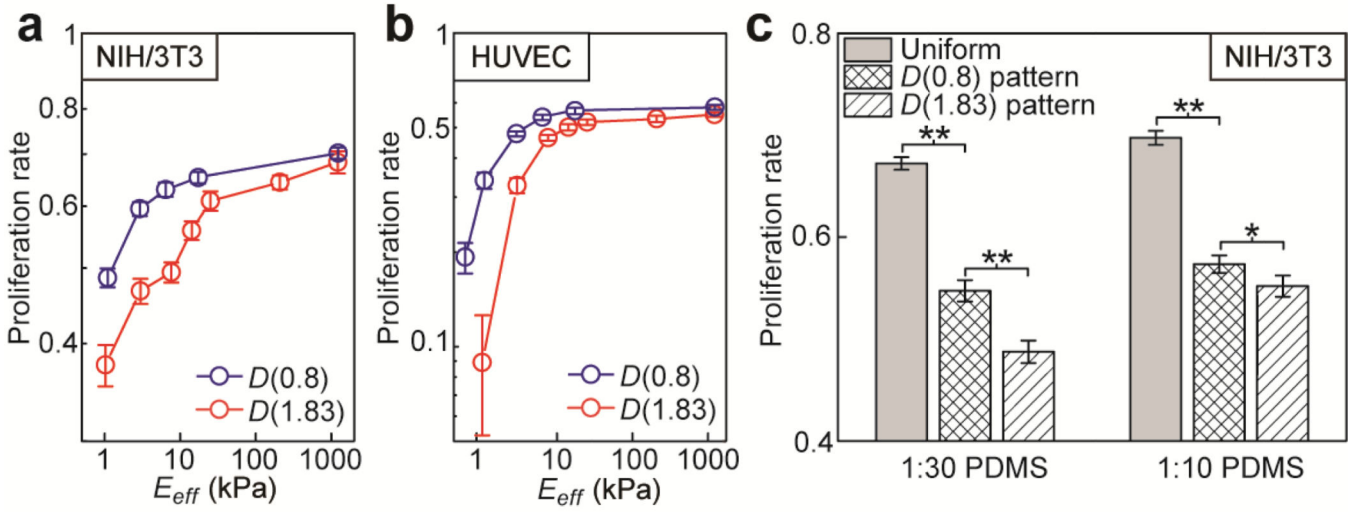

Figure 7.

Proliferation rate of NIH/3T3 and HUVECs as a function of both substrate rigidity and adhesive ECM pattern. Data are presented as the mean of three independent experiments (n=3), and error bars represent ± s.e.m. (**a&b**) Proliferation rate of NIH/3T3 (**a**) and HUVECs (**b**) as a function of the effective modulus E_{eff} of the PDMS micropost array. (**c**) Proliferation rate of NIH/3T3 plated on 1:30 (*left*) and 1:10 (*right*) flat PDMS substrates coated with different ECM patterns as indicated. *P*-values calculated using the paired student's *t*-test were indicated for statistically significant differences ($P < 0.05$ (*) and $P < 0.005$ (**)).